Title

Structural Study of Paraffin-Stabilized Methylammonium Lead Bromide Magic-Sized Clusters

Journal

The Journal of Physical Chemistry C, 127(6)

ISSN

1932-7447

Authors

Guarino-Hotz, Melissa
Barnett, Jeremy L
Chou, Kai-Chun
et al.

Publication Date

2023-02-16

DOI

10.1021/acs.jpcc.2c08645

THE JOURNAL OF PHYSICAL CHEMISTRY C
A JOURNAL OF THE AMERICAN CHEMICAL SOCIETY

pubs.acs.org/JPCC

Article

Structural Study of Paraffin-Stabilized Methylammonium Lead Bromide Magic-Sized Clusters

Melissa Guarino-Hotz, Jeremy L. Barnett, Kai-Chun Chou, Allison A. Win, Heng Zhang, Chengyu Song, Scott R. J. Oliver, and Jin Z. Zhang*

Cite This: J. Phys. Chem. C 2023, 127, 3367−3376

Read Online

ACCESS | Metrics & More | Article Recommendations | Supporting Information

ABSTRACT: Metal halide perovskites, such as methylammonium lead bromide, have recently attracted considerable attention due to their interesting and useful photoelectric properties. Here, two types of methylammonium lead bromide magic-sized clusters (MSCs), passivated with oleylamine and oleic acid, were synthesized using ligand-assisted reprecipitation (LARP) and heated LARP (HLARP) methods. The optical properties of these MSCs were characterized using UV−vis electronic absorption and photoluminescence (PL) spectroscopies. The HLARP synthesis resulted in a two-fold increase in the PL quantum yield of the MSCs to 76%. The stability of the MSCs was tested using time-dependent PL spectroscopy. LARP MSCs in solution degraded completely after 14 days under ambient conditions, while HLARP MSCs lasted for 26 days. To stabilize them, the MSCs were added to a non-coordinating matrix, paraffin. Both MSCs showed significantly improved resistance to water with the addition of paraffin. Solid LARP MSCs lost all luminescence with and without the addition of paraffin by about 3 h. Solid HLARP MSCs without paraffin started to aggregate after 3 h, but paraffin stabilized HLARP MSC films were stable for 8 days. This improved stability in solid state form allowed for accurate, nonaggregated analysis using Raman spectroscopy, X-ray diffraction, and transmission electron microscopy. Raman spectroscopy revealed that the HLARP MSCs show an additional peak at 147 cm^{-1} compared to LARP MSCs, which is attributed to methylammonium. X-ray diffraction and transmission electron microscopy confirm that MSCs have a quasi-crystalline orthorhombic structure.

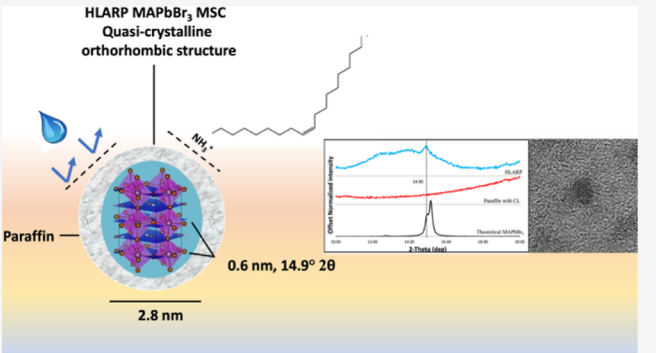

INTRODUCTION

Perovskite quantum dots (PQDs) have been studied extensively for their tunable optical properties and high photoluminescence quantum yield (PLQY).[1] Their emission window can be broadly tuned by controlling the crystal size,[2−5] capping ligand,[6,7] and elemental composition.[8,9] These fascinating optoelectronic properties make them promising materials for applications in photovoltaics for light-emitting devices,[10−12] photodetectors,[13−15] and sensing.[16−18] PQDs are characterized by their tunability, which stems from their high surface-to-volume ratio and quantum confinement.[19,20] Perovskite magic-sized clusters (MSCs) share many of these characteristics with PQDs but are smaller with higher monodispersity and narrower, bluer optical absorption and emission bands.[6,21−25] They are often described as discrete,[26] metastable intermediaries of PQDs.[27] While MSCs can be formed in a variety of ways using a variety of temperature ranges and environments, LARP is typically used for its simplicity.[28] HLARP introduces temperature variability but remains straightforward without the need for an air-free environment. Moreover, it allows the size of the nanocrystals to be tuned.[29] MSCs can be used to understand the relationship between PQDs and MSCs and provide insights into the growth mechanism of PQDs and bulk perovskite. They also present themselves as a potential material for blue-light-emitting devices.

As MSCs have a high surface-to-volume ratio, they are susceptible to instability due to surface dangling bonds or defect sites.[30−32] Thus, MSCs are typically formed using an excess concentration of capping ligand using the LARP method.[6,7,24] However, a newer synthesis utilized 15% of the capping ligand with the heated ligand-assisted reprecipitation (HLARP) method, resulting in a slightly larger particle size and more red-shifted emission.[29] Little is known about the differences between the properties of these MSCs other than their size. The change to the synthetic procedure, however, has potential stability benefits, as excess oleylamine has been

Received: December 9, 2022
Revised: January 26, 2023
Published: February 7, 2023

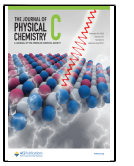

https://doi.org/10.1021/acs.jpcc.2c08645
J. Phys. Chem. C 2023, 127, 3367−3376

shown to play a role in the moisture-driven structural degradation mechanism of PQDs.[33] Oleylamine reacts with water, forming a reactive hydroxide salt that strips the 3D perovskite structure by layers, eventually forming non-emissive lead bromide.[33]

Perovskite can also degrade with light, oxygen, or water, creating a huge barrier for solid characterization and thin-film device applications.[34−40] Light and oxygen react in tandem to form free radicals that deprotonate the methylammonium cation.[37,41] Additionally, water has been shown to penetrate the perovskite structure, forming hydrate perovskite structures, and weakening the bond between the cation and lead bromide, causing degradation of the perovskite structure.[1,42] Thus, preventing the interaction of perovskite nanocrystals with light, oxygen, and water is paramount to increasing their stability.

In addition to externally driven degradation, there are various obstacles that impede the ability of perovskite MSCs to be characterized as a solid. For instance, drying effects and aggregation can make powder X-ray diffraction (PXRD) measurements difficult or inaccurate[7] and transmission electron microscopy (TEM) is often deemed inadequate due to weak contrast, poor resolution, and high beam sensitivity.[43] Therefore, little is known about their solid structure, and there is an impetus to stabilize these MSCs to glean more accurate measurements. The hydrophobic nature of paraffin has been shown to increase shelf life by creating a non-reactive hydrophobic barrier to prevent aggregation,[44,45] while the hermetic nature of paraffin seals the material from the effects of oxygen.[46]

In this work, LARP and HLARP MSCs were characterized using UV−vis electronic absorption and photoluminescent spectroscopy. We employ a simple, green, and low-cost method to encapsulate MSCs in paraffin, improving their oxygen and water stability, and allowing them to maintain their luminous intensity for longer. The stability of both HLARP and LARP MSCs was compared in solution under ambient conditions with and without paraffin and in the presence of water with and without paraffin. The samples were also dried to make films and compared with and without the presence of paraffin. LARP MSCs degraded rapidly but remained stable enough to obtain Raman data. However, UV−vis and PL results show that the HLARP MSCs' film did not aggregate or degrade for up to 8 days, allowing for analysis using both XRD and Raman spectroscopy. Moreover, HLARP MSCs proved stable enough to image nonaggregated MSCs for the first time.

EXPERIMENTAL METHODS

Materials. Methylammonium bromide (MABr, 99.9%, Greatcell Solar), lead bromide $PbBr_2$ (99.999%, Alfa Aesar), oleic acid (90%, Sigma-Aldrich), *n*-oleylamine (98.0%, Tokyo Chemical Industry), *N*,*N*-dimethylformamide (DMF, 99.9%, Fisher Scientific), paraffin wax cake (Fisher Scientific), and toluene (99.9%, Fisher Scientific) were commercially available. All chemicals were used as received without any further purification.

Synthesis of $MAPbBr_3$ MSCs. Two types of MSCs were synthesized using LARP and HLARP syntheses. MABr (1 mmol, 9.0 mg), $PbBr_2$ (1 mmol, 73.0 mg), and 400 μL of DMF were added to a borosilicate vial, and the solution was sonicated in a water bath at room temperature or between 20 °C (LARP) or 70 °C (HLARP) until all solid dissolved. Next, 0.15 mmol (HLARP) or 1 mmol (LARP) of oleic acid was added to the solution and sonicated at the same temperature for 30 s. Then, an equimolar amount of oleylamine was added to the solution and sonicated for 30 s at the same temperature. 100 μL of the precursor solution was quickly injected into 5.0 mL of toluene under vigorous stirring. The formation of these MSCs was analyzed over time (Figure S1). To stabilize the MSCs, 12 mg of paraffin was dissolved in 100 μL of the as-prepared solution. Solid samples were prepared by drop-casting the as-prepared solution and paraffin mixture onto borosilicate glass slides.

Quantum Yield. The UV−vis absorbance and fluorescence spectra of the solvent background were recorded for LARP MSCs, HLARP MSCs, and quinine sulfate. The integrated fluorescence intensity was calculated. This was repeated for five solutions with increasing concentrations (0.02, 0.04, 0.06, 0.08, and 0.10 O.D.) of LARP MSCs and HLARP MSCs. The quantum yield was then calculated using

$$QY_x = QY_{std}\left(\frac{Grad_x \times \eta_x}{Grad_{std} \times \eta_{std}}\right)$$

where x is the unknown solution, std is the standard, QY is the quantum yield, Grad is the gradient from the plot of integrated fluorescence intensity versus absorbance, and η is the refractive index of the solvent.

Stability Tests. *Open Air.* The as-prepared LARP and HLARP samples were sealed and left under ambient conditions and exposed to light and air. Aliquots of samples were removed and tested using UV−vis and PL spectroscopes over the course of 14 (LARP) to 26 days (HLARP) until the sample was no longer luminous. For paraffin stabilized samples, 12 mg of paraffin was added to 100 μL of the as-prepared solution and tested every week.

Water Stability Tests. To test water stability, 10 μL of water was added to 5 mL of as-prepared LARP and HLARP solutions. These samples were then tested using UV−vis and PL spectroscopes until they no longer emitted light. For paraffin stabilized samples, the as-prepared solution was mixed 600 mg of paraffin and similarly tested.

Solid Samples. For solid samples, 50 μL of the as-prepared sample was drop-cast onto borosilicate glass slides. This process was repeated for paraffin stabilized samples, where the as-prepared solution was mixed with 600 mg of paraffin. These samples were similarly analyzed using absorption and PL spectroscopies.

Spectroscopic Measurements. Ultraviolet−visible (UV−vis) absorption spectra were measured with an Agilent Technologies Cary 60 UV−vis spectrophotometer, and the PL spectra were measured using a Cary Eclipse spectrofluorometer using a quartz 700 μL microcuvette at room temperature and an excitation wavelength of 400 nm. Raman measurements were conducted on a Thermo Fisher DRX3 785 nm laser at a power of 1 mW for 30 s and three accumulations using a 100× objective.

X-ray Diffraction. Using the unwashed MSCs stabilized in paraffin, 50 μL were drop-cast onto a borosilicate slide and analyzed using a Rigaku American MiniFlex Plus powder diffractometer at a voltage of 40 kV and a current of 30 mA, with a scanning angle of 1.4−32 (2θ) at a rate of 0.05°/min and a step size of 0.02° over the course of 10 h.

Transmission Electron Microscopy. High-resolution transmission electron microscopy (HRTEM) and high-angle annular dark field (HAADF) scanning TEM (STEM) were performed at the National Center for Electron Microscopy

https://doi.org/10.1021/acs.jpcc.2c08645
J. Phys. Chem. C 2023, 127, 3367−3376

(NCEM) facility in Molecular Foundry, Lawrence Berkeley National Laboratory on an FEI UT Tecnai microscope, operated at an acceleration voltage of 200 kV. The sample was diluted 225-fold and dropped onto 10 nm thick lacey carbon grids. 10 μL was dropped and blotted twice and allowed to dry for 10 min before being analyzed.

RESULTS AND DISCUSSION

Optical Properties of $MAPbBr_3$ MSCs. The normalized overlayed absorption and PL spectra were measured for two types of methylammonium lead bromide MSCs synthesized by LARP and HLARP methods. In the 400−600 nm region, the LARP MSCs show a single absorption band peaked at 423 nm and a single PL band peaked at 436 nm when excited at 400 nm (Figure 1A). The HLARP MSCs exhibit red-shifted

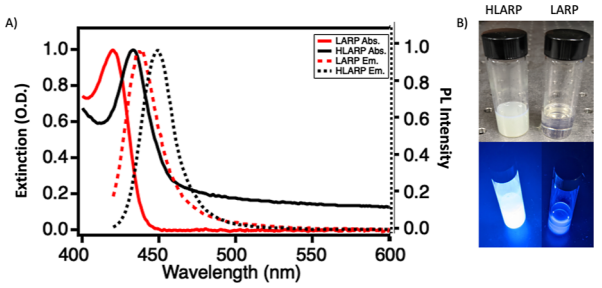

Figure 1. (A) Normalized UV−vis electronic absorption and PL spectra for LARP and HLARP syntheses and (B) images of MSCs made with LARP and HLARP under ambient light and UV light.

absorption and PL bands peaked at 432 and 450 nm, respectively. This red shift of both the absorption and PL bands indicates the formation of larger MSCs and is in good agreement with previous reports.[7,29] The PL bands of both samples have a narrow full width at half maximum of 20 nm, indicative of a narrow size distribution.

The PLQY was obtained by comparing to quinine sulfate. HLARP MSCs have a PLQY of 76%, over double that of the LARP MSCs at 36%. This is expected as higher temperature syntheses, such as those in PQD hot injection, often lead to nanoparticles with higher PLQY (Figure 1B).[47,48] Moreover, HLARP MSCs' absorption band is 10 times as intense as LARP MSCs' (Figure S1), showing an increase in concentration and product yield. The increased temperature leads to more collisions, increasing the number of nucleation sites and the rate of the reaction.[29] Thus, the HLARP synthesis produces a more concentrated solution of MSCs with higher PLQYs.

Stability Analysis. The long-term stability of MSCs in solution was monitored until the sample fully degraded and lost luminous intensity (Figure 2). The time-dependent PL spectra of LARP MSCs under ambient conditions indicate that they retain their 436 nm emission without shifting but completely degrade after 14 days (Figure 2A). The time-dependent PL spectra of HLARP MSCs under similar ambient conditions show that the HLARP MSCs have ∼20 times the initial PL emission intensity of LARP MSCs but show a different degradation mechanism (Figure 2B). The initial emission band starts at 450 nm and shifts to 456 nm after 24 h. This indicates that the MSCs are growing slightly due to Ostwald ripening and reaching a larger metastable state.[49−51] The intensity of the solution increases for up to 5 days, more than doubling in intensity before starting to diminish and degrade. This is likely due to leftover starting reagents in the unwashed solution forming new nucleation sites and thus new MSCs and is similarly reflected in the absorption spectra (Figure S2). The leftover capping ligand in the solution does not appear to be a detriment at this concentration, as HLARP MSCs take 26 days to fully diminish. Both degradation processes plotted over time show the increased stability of HLARP over LARP MSCs in ambient conditions (Figure 2G).

MSCs can degrade due to water, light, oxygen, or excess capping ligand.[42] The only difference between the LARP and HLARP MSCs is their size and the amount of capping ligand leftover in the solution. In general, larger nanoparticles show increased stability over smaller nanoparticles, at least partially justifying HLARP's improved stability.[51] Additionally, LARP MSCs are synthesized with 667% more capping ligands than the HLARP synthesis. Since oleic acid and oleylamine were used as stabilizing ligands and they readily react with each other, this may result in the reaction of bound and unbound ligands, causing the detachment of bound ligands, and resulting in aggregation of the nanoparticles.[52] Second, oleylamine can react with water to form oleyl ammonium salt, which reacts and causes a moisture-induced structural degradation.[33] Therefore, increasing the amount of oleylamine in the solution leaves MSCs more susceptible to water destabilization. By synthesizing HLARP MSCs with less capping ligands, they do not undergo these capping ligand degradations as readily and are less susceptible to the oleylamine moisture-driven degradation, making them more stable under ambient conditions. HLARP MSCs stabilized in paraffin remain stable for at least 3 months under ambient conditions (Figure S3).

To further test the stability and resilience against humidity, 10 μL of water was injected into the 5.0 mL as-prepared sample. The LARP MSCs with this addition proved to be highly unstable in water, as the time-dependent PL spectra fully diminished in 4 min (Figure 2C). In comparison, the time-dependent PL spectra of HLARP MSCs showed they remained luminous for 30 min (Figure 2D). Typically, when water molecules in the air interact with the perovskite crystal, strong hydrogen bonds form with the organic cations, weakening the bond between the cation and $PbBr_2$, allowing for faster deprotonation of the organic cation, leaving the crystal more susceptible to external stressors.[42,53] Moreover, as stated above, the excess oleylamine can react with water to speed up moisture-driven structural degradation.[33]

To reduce degradation, paraffin was introduced as a non-coordinating solvent and stabilizing matrix.[54] Long-chain hydrophobic polymers have been shown to greatly increase water stability by preventing the interaction between water and the PQDs.[55] Here, we see significant improvements to the stability of MSCs with the addition of paraffin. The time-dependent PL spectra of the LARP MSCs show that the MSCs remained luminous for nearly seven times longer, retaining PL for 27 min (Figure 2E). The time-dependent PL spectra of the paraffin stabilized HLARP MSCs also show an improvement and emitted for over 90 min (Figure 2F).

Paraffin has been shown to aid PQDs largely with water degradation and partially with oxygen degradation, acting as a hermetic barrier.[46,53−55] With the addition of water, LARP MSCs shifted from 436 to 423 nm before the PL intensity diminished. This indicates that the MSCs are breaking into smaller particles before losing luminescence. In the case of the HLARP MSCs, the longevity of the MSCs is improved by a factor of about three. HLARP MSCs degraded without

https://doi.org/10.1021/acs.jpcc.2c08645
J. Phys. Chem. C 2023, 127, 3367−3376

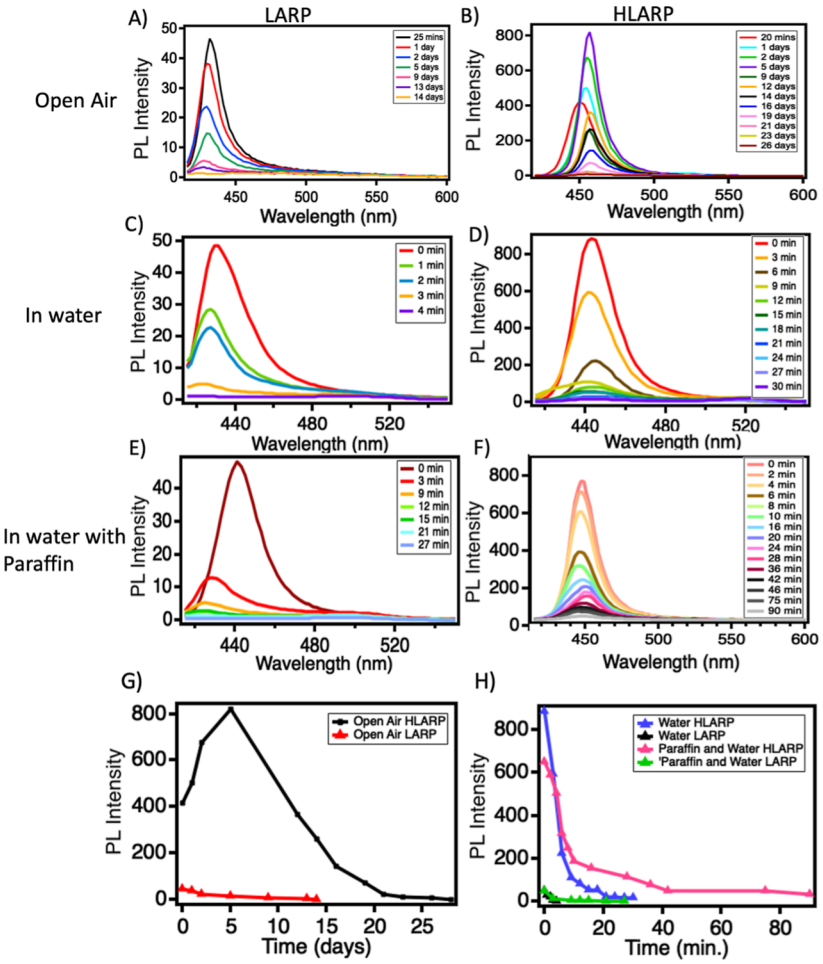

Figure 2. Time-dependent PL stability analysis of LARP and HLARP: (A) LARP MSCs under ambient conditions, exposed to light and air; (B) HLARP MSCs under ambient conditions, exposed to light and air; (C) LARP MSCs after the addition of 10 μL of water; (D) HLARP MSCs after the addition of 10 μL of water; (E) LARP MSCs after the stabilization in paraffin and the addition of 10 μL of water; (F) HLARP MSCs after the stabilization in paraffin and the addition of 10 μL of water; (G) PL intensity over time comparing LARP and HLARP MSCs under ambient conditions; and (H) PL intensity over time comparing LARP and HLARP MSCs with the addition of water.

exhibiting peak-shifting and retained their 450 nm emission. The small addition of water significantly increases the degradation of the MSCs. Both LARP and HLARP MSCs retain their PL on the scale of weeks when exposed to light and air, but the addition of water, even in the presence of a stabilizing matrix, degrades them in a matter of minutes. Thus, water degradation appears to be the main cause of structural degradation. The addition of paraffin significantly improved the stability and shelf life of these materials and facilitated their characterization in solution. The comparison of the diminishing PL intensities due to water degradation is shown in Figure 2H (corresponding absorption spectra, Figure S2).

For applications and structural characterizations, it is important for the MSCs to be stabilized as a solid. However, MSCs degrade in the solid form as particles aggregate or fall apart upon drying due to local supersaturation.[43,56,57] The LARP MSCs were drop-cast onto borosilicate glass slides and analyzed after 3 h. Their PL spectrum was indistinguishable from the borosilicate background, retaining no luminescence (Figure S4). To stabilize the LARP MSCs, paraffin was added prior to drop-casting. Similarly, after 3 h, the LARP MSCs lost all luminosity. Excess capping ligands could severely limit the ability of these nanoparticles to stabilize as a solid. Thus, if the smaller sized LARP MSCs are desirable for applications, washing protocols may improve stability.

The PL spectra of HLARP MSCs in solution and their dried counterparts were compared, as shown in Figure 3. The solution PL spectrum has one band peaked at 450 nm, while the dried HLARP MSCs without paraffin have the same band with a peak at 450 nm, but with a new band appearing at 473 nm (Figure 3A), indicative of the formation of larger particles.[29] One can observe the lighter blue tint starting to

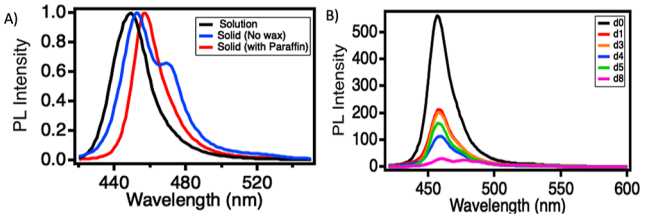

Figure 3. Stability of HLARP MSCs as a solid, determined by PL intensity of (A) normalized spectra of the solution compared to as-prepared dried HLARP MSCs and dried HLARP MSCs stabilized in paraffin after 3 h and (B) paraffin stabilized HLARP MSCs over 8 days.

https://doi.org/10.1021/acs.jpcc.2c08645
J. Phys. Chem. C 2023, 127, 3367−3376

form on the film (Figure S4). However, with the addition of paraffin, the MSCs keep the one emission band but shift slightly from 450 to 456 nm (Figure 3A). This is the same shift that was seen in the solution after 1 day, attributed to slightly more stable and larger MSCs after possible Ostwald ripening.[58] The paraffin-stabilized HLARP MSC film was left under ambient conditions and remained stable for 8 days (Figure 3B). This is important for their potential device applications and characterization in solid state form (corresponding absorption data, Figure S5).

Structural Analysis. The Raman spectra in high-frequency and low-frequency regions were measured for the solid LARP and HLARP MSCs, immediately upon drying and before aggregation, as shown in Figure 4. In the high-frequency region

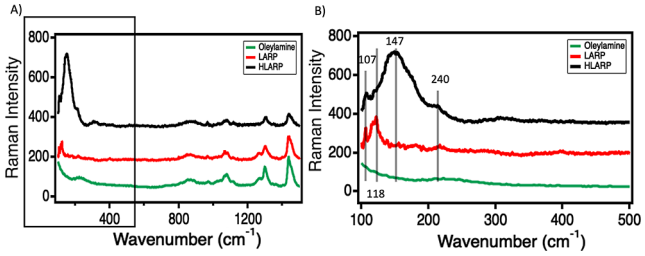

Figure 4. Comparison of oleylamine, LARP MSCs, and HLARP MSCs using: (A) high- and low-frequency Raman spectra and (B) zoomed in low-frequency Raman spectra.

above 700 cm^{-1}, both LARP and HLARP confirm the presence of the primary capping ligand, oleylamine (Figure 4A).[59] All modes in the low-frequency region are in good agreement with methylammonium lead bromide bulk perovskite (Figure 4B). The peaks at 107 and 118 cm^{-1} are indicative of lurching methylammonium, and the broad peak at 240 cm^{-1} due to torsional vibration of methylammonium is present in both LARP and HLARP. However, the 147 cm^{-1} nodding donkey around C is prominent and only shown in the HLARP MSCs.[60] This mode corresponds to a rotational vibration of the cation around the methylammonium carbon and is presumably affected by octahedra tilting. The distortions of the crystal lattice are due to the hydrogen bonding with the halogen and thus provide some measure of the coupling between the molecule and the inorganic framework. The presence of this mode in the HLARP MSCs, and not the LARP MSCs, suggests that the larger MSC is more ordered and that upon the growth of the nanocrystal, the methylammonium becomes more firmly bound in the nanocrystal due to a distortion of the framework.[61] This distortion could play a role in the improved stability of HLARP MSCs over LARP MSCs.

Paraffin stabilization of the HLARP MSCs allowed for PXRD analysis. The stability of the HLARP MSC film was confirmed using PL spectroscopy and the XRD patterns of HLARP MSCs are shown in Figure 5. Sharp peaks at ∼ 2, 4, 6.5, 21.5, and 23.9° (2θ) due to paraffin are observed. Broad features at 12.4, 13.8, and 14.9° (2θ) are attributed to HLARP MSCs. The distinct peak at 14.9° correlates well with the expected (020) plane of the orthorhombic $MAPbBr_3$ perovskite. This peak is further confirmed by the higher order amorphous hump (∼26−31.5° 2θ) (Figure S5). Paraffin with oleylamine and oleic acid capping ligands dried in a similar manner produce no features in the 12−15° area of interest. The diffraction data of the HLARP MSCs share common perovskite *d*-spacings and likely have a distorted perovskite structure. The 14.9° peak is slightly shifted toward a smaller 2θ. This indicated the shift to larger *d*-spacings from the theoretical 14.95° (5.92 Å) peak of the orthorhombic $MAPbBr_3$. Moreover, the peak is significantly broader, indicating its smaller size.[62] Organic ligand passivation can cause lattice strain near the surface, which typically relaxes within a few monolayers.[63] However, due to the small size of MSCs, there are likely five (020) lattice planes. Since their size is so small, ligand passivation at the surface strains most of the MSCs' perovskite structure, which would similarly agree with the broad diffraction peaks. Given that LARP MSCs show less order in their low-frequency Raman spectra, it is likely that LARP MSCs would show even less crystalline character. This is further supported by their estimated smaller size since larger nanocrystals have more layers to satisfy Bragg's law and produce sharper reflections with increased intensity.[64]

HRTEM images of HLARP MSCs (Figure 6) indicate that the average size was 2.46 ± 0.15 nm by 3.20 ± 0.19, for an average of 2.8 nm, smaller than anticipated with the Brus method.[29] Moreover, the MSCs shown here are around 2 nm smaller than previous reports of TEM images where aggregation was not prevented.[7] These measurements indicate that the MSCs have low crystallinity. The fast Fourier transform of the HRTEM reveals a lattice spacing of ∼0.30 nm, which is consistent with the (040) Miller index (Figure

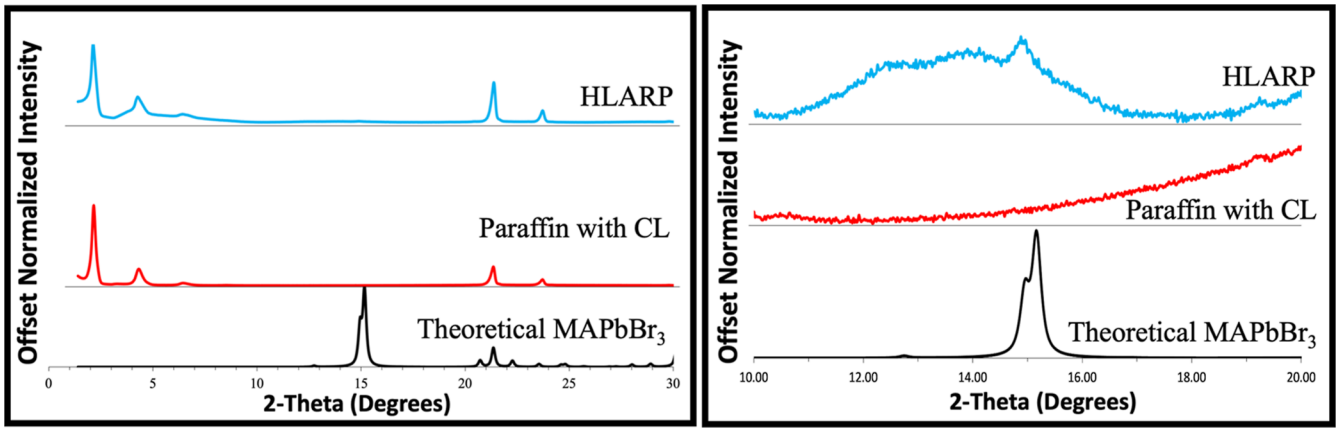

Figure 5. XRD patterns for HLARP MSCs, paraffin and capping ligand, and theoretical spectrum of methylammonium lead bromide (left) from 0 to 30° (right) from 10 to 20°.

https://doi.org/10.1021/acs.jpcc.2c08645
J. Phys. Chem. C 2023, 127, 3367−3376

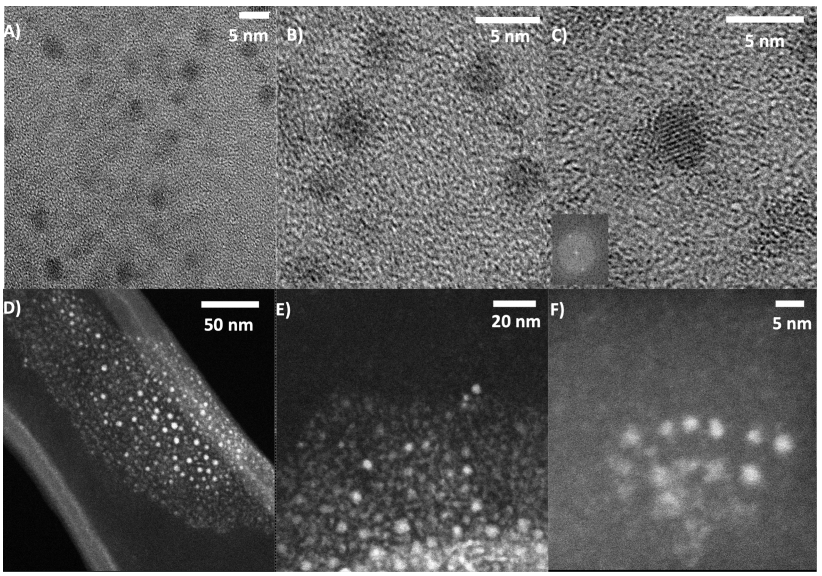

Figure 6. Images of HLARP MSCs at various resolutions using: (A–C) HRTEM and (D–F) HAADF STEM.

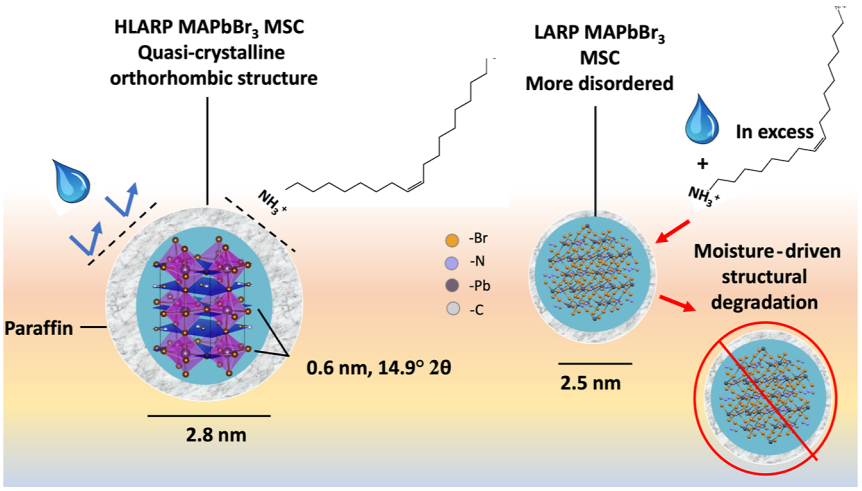

Figure 7. Scheme illustration of the differences between LARP and HLARP MSCs and the major effects on their stabilization.

6C). Every two lattice spacings are consistent with the (020) Miller index, a *d*-spacing of ∼0.6 nm, and the 14.9° diffraction peak in the PXRD (Figure 6C). The (040) with a 2θ of ∼30° is represented as a very broad and weakly diffracting reflection (Figure S5). Both (020) and (040) miller indices are indicative of the orthorhombic crystal structure.[62,65] The TEM image shows lattice planes perpendicular to the *b*-axis lattice constant (Figure 6C). The *b* axis is approximately 1.5 times longer than a or *c* axes, which correlates with the shape of the MSCs. The lattice spacing is not present in all the images, likely due to beam sensitivity and particle movement. This makes it hard to characterize the other spacings exactly and also explains the broadness shown in the PXRD pattern. Lattice spacings of around 0.36 nm are also present, which could account for the 12.4° powder peak, but there are very few layers to concretely determine this.

If the concentration is too high, some MSCs aggregate into PQDs (Figure S7). These nanoparticles are ∼5 nm in size and show much higher crystallinity by contrast. They show lattice spacings of 0.30 and 0.25 nm, which are in good agreement with the theoretical methylammonium lead bromide powder pattern. Thus, it is possible to structurally distinguish between MSCs and PQDs. MSCs have perovskite characteristics but are quasi-crystalline. PQDs show higher crystallinity and therefore are more similar to the perovskite crystal structure.

A potential mechanism of paraffin stabilization and a model of a quasi-crystalline $MAPbBr_3$ LARP and HLARP MSCs can be hypothesized (Figure 7). The HLARP and LARP MSCs differ in many characteristics. While the HLARP MSCs are slightly harder to make, they possess double the PLQY of the LARP MSCs. The LARP MSCs' decrease in PLQY could be due to an increased number of defects or trap states which give alternative pathways to radiative recombination and can significantly decrease the quantum yield.[8,66−69] This would be contrary to previous hypotheses surrounding the LARP and HLARP MSCs.[29] Additionally, the LARP MSCs were estimated to be around 3.04 nm in size using the Brus model.[29] However, using TEM, it was determined that the larger HLARP MSCs are an average of 2.8 nm in size. Therefore, by modifying the Brus approximation methods, LARP MSCs are likely 2.5 nm in size (Figure 7).[24] This smaller size could lead to their relative instability.[51] In contrast,

https://doi.org/10.1021/acs.jpcc.2c08645
J. Phys. Chem. C 2023, 127, 3367−3376

the HLARP MSCs are formed using a minimal amount of capping ligand at an elevated temperature. This extra step not only increases the particle size to 2.8 nm but also doubles the PLQY to 76%. The increase could be due to the higher temperature, providing sufficient energy to allow the MSCs to reach a more stable state. The HLARP MSCs' improved stability allowed them to be characterized with PXRD and TEM. They show lattice spacings of 0.30 nm, which suggest that they are orthorhombic (Figure 7). Contrastingly, the instability of the LARP MSCs hindered their ability to be characterized as a solid.

LARP and HLARP MSCs also differ in the capping ligand concentration during synthesis and the order within their structures. LARP MSCs are synthesized with 667% more capping ligands. Excess capping ligands have been shown to play a key role in the degradation of MSCs. There are two potential mechanisms. Since there are both free acid and amine ligands present in the solution, they have the ability to react with ligands bound on the surface of the MSC, leading to aggregation.[52] Furthermore, oleylamine has been shown to react strongly with water and provide a mechanism for moisture-driven structural degradation (Figure 7).[33] This likely contributes to the increased instability of LARP MSCs over HLARP MSCs. Thus, to improve the stability of the LARP synthesis, washing protocols must be optimized.

HLARP MSCs are also more crystalline than LARP MSCs, suggested by the additional Raman mode at 147 cm^{-1}. This indicates an additional bond between the methylammonium and the inorganic framework. Water molecules destabilize perovskite crystal structures by binding to their organic cation and weakening its bond to the crystal structure.[37] The HLARP MSCs are more resilient to water and excess capping ligand degradation, likely due to their increased structural order. Using paraffin as a stabilizing matrix, the HLARP MSCs were stable for 8 days as a solid and over 3 months in solution exposed to light, oxygen, and water. This is likely due to the hermetic nature of paraffin providing a barrier to these destabilizing agents. Moreover, with the introduction of a matrix, paraffin could potentially inhibit the interaction of unbound capping ligands with the material. These data suggest that MSCs can be stabilized for future applications in photonics in similar ways to quantum dots.

CONCLUSIONS

Two types of methylammonium lead bromide MSCs, passivated with oleylamine and oleic acid, were synthesized using LARP and HLARP methods. These MSCs were characterized using UV−vis electronic absorption and PL spectroscopy. The HLARP synthesis resulted in an increase in the PLQY of the MSCs by two-fold to 76% and showed increased product yield. The stability of the MSCs was tested using time-dependent PL spectroscopy. LARP MSCs in solution degraded completely after 14 days under ambient conditions, while HLARP MSCs lasted for 26 days. To stabilize them, the MSCs were added to paraffin to create a hydrophobic and hermetic barrier and protect them from the degrading effects of water and oxygen. Both paraffin-stabilized MSCs showed increased resilience to the addition of water. Solid LARP MSCs lost all luminescence with and without the addition of paraffin by about 3 h. Solid HLARP MSCs without paraffin started to aggregate after 3 h, but paraffin-stabilized HLARP MSC films were stable for 8 days. This improved stability in solid state form allowed for analysis using Raman spectroscopy, PXRD, and TEM. Raman spectroscopy revealed that the HLARP MSCs show an additional peak at 147 cm^{-1} compared to LARP MSCs, which is attributed to methylammonium, indicate a more highly ordered structure, and may have implications in HLARP's increased stability. PXRD and TEM confirm that MSCs have a quasi-crystalline orthorhombic structure. The significantly extended stability of the solid HLARP MSCs with paraffin shows promise for future use in photonics.

ASSOCIATED CONTENT

Supporting Information

The Supporting Information is available free of charge at https://pubs.acs.org/doi/10.1021/acs.jpcc.2c08645.

UV−vis and PL spectra of the formation of LARP and HLARP MSCs; UV−vis spectra of LARP and HLARP MSCs over time in ambient conditions, with the addition of water, and with the addition of water and paraffin; UV−vis and PL spectra of HLARP MSCs in solution after 1 day and after 90 days; PL spectra of glass, dried LARP MSCs after 3 h without paraffin, and dried LARP MSCs after 3 h with paraffin, UV−vis spectra of HLARP MSCs in solution, dried without paraffin, and dried with paraffin, and dried with paraffin over 8 days; PXRD pattern of HLARP MSCs, paraffin with capping ligands, and theoretical $MAPbBr_3$; and HRTEM images of PQDs and MSCs (PDF)

AUTHOR INFORMATION

Corresponding Author

Jin Z. Zhang − *Department of Chemistry and Biochemistry, University of California, Santa Cruz, California 95064, United States;* orcid.org/0000-0003-3437-912X; Email: zhang@ucsc.edu

Authors

Melissa Guarino-Hotz − *Department of Chemistry and Biochemistry, University of California, Santa Cruz, California 95064, United States;* orcid.org/0000-0001-6310-8156

Jeremy L. Barnett − *Department of Chemistry and Biochemistry, University of California, Santa Cruz, California 95064, United States*

Kai-Chun Chou − *Department of Chemistry and Biochemistry, University of California, Santa Cruz, California 95064, United States*

Allison A. Win − *Department of Chemistry and Biochemistry, University of California, Santa Cruz, California 95064, United States;* orcid.org/0000-0001-7867-1953

Heng Zhang − *Department of Chemistry and Biochemistry, University of California, Santa Cruz, California 95064, United States*

Chengyu Song − *National Center of Electron Microscopy, Molecular Foundry, Lawrence Berkeley National Laboratory, Berkeley, California 94720, United States*

Scott R. J. Oliver − *Department of Chemistry and Biochemistry, University of California, Santa Cruz, California 95064, United States;* orcid.org/0000-0002-6160-1518

Complete contact information is available at: https://pubs.acs.org/10.1021/acs.jpcc.2c08645

https://doi.org/10.1021/acs.jpcc.2c08645
J. Phys. Chem. C 2023, 127, 3367−3376

Author Contributions

The manuscript was written through contributions of all authors. All authors have given approval to the final version of the manuscript.

Notes

The authors declare no competing financial interest.

■ ACKNOWLEDGMENTS

This work was supported by NASA (MACES, grant no. NNX15AQ01A). We acknowledge the assistance of the X-ray Facility at University of California Santa Cruz for the use of the Rigaku SmartLab diffractometer, funded by NSF MRI grant number 1126845. Work at the Molecular Foundry was supported by the Office of Science, Office of Basic Energy Sciences, the U.S. Department of Energy, under contract no. DE-AC02-05CH11231.

■ REFERENCES

(1) Wang, H.-C.; Bao, Z.; Tsai, H.-Y.; Tang, A.-C.; Liu, R.-S. Perovskite Quantum Dots and Their Application in Light-Emitting Diodes. *Small* **2018**, *14*, 1702433.

(2) Leng, J.; Wang, T.; Zhao, X.; Ong, E. W. Y.; Zhu, B.; Ng, J. D. A.; Wong, Y.-C.; Khoo, K. H.; Tamada, K.; Tan, Z.-K. Thermodynamic Control in the Synthesis of Quantum-Confined Blue-Emitting $CsPbBr_3$ Perovskite Nanostrips. *J. Phys. Chem. Lett.* **2020**, *11*, 2036−2043.

(3) Peighambardoust, N. S.; Sadeghi, E.; Aydemir, U. Lead Halide Perovskite Quantum Dots for Photovoltaics and Photocatalysis: A Review. *ACS Appl. Nano Mater.* **2022**, *5*, 14092−14132.

(4) Li, H.; Lu, W.; Zhao, G.; Song, B.; Dong, W.; Han, G. Synthesis of Size-Controllable Self-Assembled $CsPbBr_3$ Perovskite Nanowires: Implications for Photoemission with Less Recombination. *ACS Appl. Nano Mater.* **2022**, *5*, 5527−5534.

(5) Chen, X.; Peng, L.; Huang, K.; Shi, Z.; Xie, R.; Yang, W. Non-Injection Gram-Scale Synthesis of Cesium Lead Halide Perovskite Quantum Dots with Controllable Size and Composition. *Nano Res.* **2016**, *9*, 1994−2006.

(6) Xu, K.; Allen, A. C.; Luo, B.; Vickers, E. T.; Wang, Q.; Hollingsworth, W. R.; Ayzner, A. L.; Li, X.; Zhang, J. Z. Tuning from Quantum Dots to Magic Sized Clusters of $CsPbBr_3$ Using Novel Planar Ligands Based on the Trivalent Nitrate Coordination Complex. *J. Phys. Chem. Lett.* **2019**, *10*, 4409−4416.

(7) Liu, L.; Xu, K.; Vickers, E. T.; Allen, A.; Li, X.; Peng, L.; Zhang, J. Z. Varying the Concentration of Organic Acid and Amine Ligands Allows Tuning between Quantum Dots and Magic-Sized Clusters of $CH_3NH_3PbBr_3$ Perovskite: Implications for Photonics and Energy Conversion. *ACS Appl. Nano Mater.* **2020**, *3*, 12379−12387.

(8) Lou, Y.; Fang, M.; Chen, J.; Zhao, Y. Formation of Highly Luminescent Cesium Bismuth Halide Perovskite Quantum Dots Tuned by Anion Exchange. *Chem. Commun.* **2018**, *54*, 3779−3782.

(9) Wang, H.; Sui, N.; Bai, X.; Zhang, Y.; Rice, Q.; Seo, F. J.; Zhang, Q.; Colvin, V. L.; Yu, W. W. Emission Recovery and Stability Enhancement of Inorganic Perovskite Quantum Dots. *J. Phys. Chem. Lett.* **2018**, *9*, 4166−4173.

(10) Wei, Y.; Cheng, Z.; Lin, J. An Overview on Enhancing the Stability of Lead Halide Perovskite Quantum Dots and Their Applications in Phosphor-Converted LEDs. *Chem. Soc. Rev.* **2019**, *48*, 310−350.

(11) Wang, S.; Wang, Y.; Zhang, Y.; Zhang, X.; Shen, X.; Zhuang, X.; Lu, P.; Yu, W. W.; Kershaw, S. V.; et al. Cesium Lead Chloride/Bromide Perovskite Quantum Dots with Strong Blue Emission Realized via a Nitrate-Induced Selective Surface Defect Elimination Process. *J. Phys. Chem. Lett.* **2019**, *10*, 90−96.

(12) Singh, R. K.; Sharma, P.; Kumar, R.; Som, S.; Dutta, S.; Jain, N.; Chaurasiya, R.; Meena, M. L.; Ho, J.-S.; Dai, S.-W.; et al. $CH_3NH_3Pb_{1-X}CoxBr_{3-2x}Cl_{2x}$ Perovskite Quantum Dots for Wide-Color Backlighting. *ACS Appl. Nano Mater.* **2021**, *4*, 717−728.

(13) Bi, C.; Kershaw, S. V.; Rogach, A. L.; Tian, J. Improved Stability and Photodetector Performance of $CsPbI_3$ Perovskite Quantum Dots by Ligand Exchange with Aminoethanethiol. *Adv. Funct. Mater.* **2019**, *29*, 1902446.

(14) Zhang, Z.-X.; Li, C.; Lu, Y.; Tong, X.-W.; Liang, F.-X.; Zhao, X.-Y.; Wu, D.; Xie, C.; Luo, L.-B. Sensitive Deep Ultraviolet Photodetector and Image Sensor Composed of Inorganic Lead-Free $Cs_3Cu_2I_5$ Perovskite with Wide Bandgap. *J. Phys. Chem. Lett.* **2019**, *10*, 5343−5350.

(15) Tang, J.-F.; Sie, Y.-D.; Tseng, Z.-L.; Lin, J.-H.; Chen, L.-C.; Hsu, C.-L. Perovskite Quantum Dot−ZnO Nanowire Composites for Ultraviolet−Visible Photodetectors. *ACS Appl. Nano Mater.* **2022**, *5*, 7237−7245.

(16) Lu, L.-Q.; Tan, T.; Tian, X.-K.; Li, Y.; Deng, P. Visual and Sensitive Fluorescent Sensing for Ultratrace Mercury Ions by Perovskite Quantum Dots. *Anal. Chim. Acta* **2017**, *986*, 109−114.

(17) Wang, Y.; Zhu, Y.; Huang, J.; Cai, J.; Zhu, J.; Yang, X.; Shen, J.; Jiang, H.; Li, C. $CsPbBr_3$ Perovskite Quantum Dots-Based Monolithic Electrospun Fiber Membrane as an Ultrastable and Ultrasensitive Fluorescent Sensor in Aqueous Medium. *J. Phys. Chem. Lett.* **2016**, *7*, 4253−4258.

(18) Shan, H.; Xuan, W.; Li, Z.; Hu, D.; Gu, X.; Huang, S. Room-Temperature Hydrogen Sulfide Sensor Based on Tributyltin Oxide Functionalized Perovskite $_{CsPbBr3}$ Quantum Dots. *ACS Appl. Nano Mater.* **2022**, *5*, 6801−6809.

(19) Tyagi, P.; Arveson, S. M.; Tisdale, W. A. Colloidal Organohalide Perovskite Nanoplatelets Exhibiting Quantum Confinement. *J. Phys. Chem. Lett.* **2015**, *6*, 1911−1916.

(20) Dong, Y.; Qiao, T.; Kim, D.; Parobek, D.; Rossi, D.; Son, D. H. Precise Control of Quantum Confinement in Cesium Lead Halide Perovskite Quantum Dots via Thermodynamic Equilibrium. *Nano Lett.* **2018**, *18*, 3716−3722.

(21) Stein, J. L.; Steimle, M. I.; Terban, M. W.; Petrone, A.; Billinge, S. J. L.; Li, X.; Cossairt, B. M. Cation Exchange Induced Transformation of InP Magic-Sized Clusters. *Chem. Mater.* **2017**, *29*, 7984−7992.

(22) Xu, K.; Vickers, E. T.; Luo, B.; Allen, A. C.; Chen, E.; Roseman, G.; Wang, Q.; Kliger, D. S.; Millhauser, G. L.; Yang, W.; et al. First Synthesis of Mn-Doped Cesium Lead Bromide Perovskite Magic Sized Clusters at Room Temperature. *J. Phys. Chem. Lett.* **2020**, *11*, 1162−1169.

(23) Liu, L.; Pan, K.; Xu, K.; Zhang, J. Z. Impact of Molecular Ligands in the Synthesis and Transformation between Metal Halide Perovskite Quantum Dots and Magic Sized Clusters. *ACS Phys. Chem. Au* **2022**, *2*, 156−170.

(24) Vickers, E. T.; Chen, Z.; Cherrette, V.; Smart, T.; Zhang, P.; Ping, Y.; Zhang, J. Z. Interplay between Perovskite Magic-Sized Clusters and Amino Lead Halide Molecular Clusters. *Research* **2021**, *2021*, 6047971.

(25) Vickers, E. T.; Xu, K.; Dreskin, B. W.; Graham, T. A.; Li, X.; Zhang, J. Z. Ligand Dependent Growth and Optical Properties of Hybrid Organo-Metal Halide Perovskite Magic Sized Clusters. *J. Phys. Chem. C* **2019**, *123*, 18746−18752.

(26) Pun, A. B.; Mazzotti, S.; Mule, A. S.; Norris, D. J. Understanding Discrete Growth in Semiconductor Nanocrystals: Nanoplatelets and Magic-Sized Clusters. *Acc. Chem. Res.* **2021**, *54*, 1545−1554.

(27) Jiang, Z.-J.; Kelley, D. F. Role of Magic-Sized Clusters in the Synthesis of CdSe Nanorods. *ACS Nano* **2010**, *4*, 1561−1572.

(28) Dagtepe, P.; Chikan, V.; Jasinski, J.; Leppert, V. J. Quantized Growth of CdTe Quantum Dots; Observation of Magic-Sized CdTe Quantum Dots. *J. Phys. Chem. C* **2007**, *111*, 14977−14983.

(29) Guarino-Hotz, M.; Barnett, J. L.; Pham, L. B.; Win, A. A.; Cherrette, V. L.; Zhang, J. Z. Tuning between Methylammonium Lead Bromide Perovskite Magic-Sized Clusters and Quantum Dots through Ligand Assisted Reprecipitation at Elevated Temperatures. *J. Phys. Chem. C* **2022**, *126*, 13854−13862.

(30) Nevers, R.; Hanrath, B.; Robinson, T.; Robinson, D. Surface Chemistry of Cadmium Sulfide Magic-Sized Clusters: A Window into

https://doi.org/10.1021/acs.jpcc.2c08645
J. Phys. Chem. C 2023, 127, 3367−3376

Ligand-Nanoparticle Interactions. *Chem. Commun.* **2017**, *53*, 2866−2869.
(31) Zhang, J. Z. A "Cocktail" Approach to Effective Surface Passivation of Multiple Surface Defects of Metal Halide Perovskites Using a Combination of Ligands. *J. Phys. Chem. Lett.* **2019**, *10*, 5055−5063.
(32) Suh, Y.-H.; Kim, T.; Choi, J. W.; Lee, C.-L.; Park, J. High-Performance CsPbX3 Perovskite Quantum-Dot Light-Emitting Devices via Solid-State Ligand Exchange. *ACS Appl. Nano Mater.* **2018**, *1*, 488−496.
(33) Sandeep, K.; Gopika, K. Y.; Revathi, M. R. Role of Capped Oleyl Amine in the Moisture-Induced Structural Transformation of $CsPbBr_3$ Perovskite Nanocrystals. *Phys. Status Solidi RRL* **2019**, *13*, 1900387.
(34) Kim, Y.; Yassitepe, E.; Voznyy, O.; Comin, R.; Walters, G.; Gong, X.; Kanjanaboos, P.; Nogueira, A. F.; Sargent, E. H. Efficient Luminescence from Perovskite Quantum Dot Solids. *ACS Appl. Mater. Interfaces* **2015**, *7*, 25007−25013.
(35) Ouyang, Y.; Li, Y.; Zhu, P.; Li, Q.; Gao, Y.; Tong, J.; Shi, L.; Zhou, Q.; Ling, C.; Chen, Q.; et al. Photo-Oxidative Degradation of Methylammonium Lead Iodide Perovskite: Mechanism and Protection. *J. Mater. Chem. A* **2019**, *7*, 2275−2282.
(36) Shirayama, M.; Kato, M.; Miyadera, T.; Sugita, T.; Fujiseki, T.; Hara, S.; Kadowaki, H.; Murata, D.; Chikamatsu, M.; Fujiwara, H. Degradation Mechanism of $CH_3NH_3PbI_3$ Perovskite Materials upon Exposure to Humid Air. *J. Appl. Phys.* **2016**, *119*, 115501.
(37) Abdelmageed, G.; Jewell, L.; Hellier, K.; Seymour, L.; Luo, B.; Bridges, F.; Zhang, J. Z.; Carter, S. Mechanisms for Light Induced Degradation in $MAPbI_3$ Perovskite Thin Films and Solar Cells. *Appl. Phys. Lett.* **2016**, *109*, 233905.
(38) Kundu, S.; Kelly, T. L. In Situ Studies of the Degradation Mechanisms of Perovskite Solar Cells. *EcoMat* **2020**, *2*, No. e12025.
(39) Li, B.; Li, Y.; Zheng, C.; Gao, D.; Huang, W. Advancements in the Stability of Perovskite Solar Cells: Degradation Mechanisms and Improvement Approaches. *RSC Adv.* **2016**, *6*, 38079−38091.
(40) Zhao, Y.; Xie, C.; Zhang, X.; Yang, P. $CsPbX_3$ Quantum Dots Embedded in Zeolitic Imidazolate Framework-8 Microparticles for Bright White Light-Emitting Devices. *ACS Appl. Nano Mater.* **2021**, *4*, 5478−5485.
(41) Bryant, D.; Aristidou, N.; Pont, S.; Sanchez-Molina, I.; Chotchunangatchaval, T.; Wheeler, S.; Durrant, R.; Haque, A. Light and Oxygen Induced Degradation Limits the Operational Stability of Methylammonium Lead Triiodide Perovskite Solar Cells. *Energy Environ. Sci.* **2016**, *9*, 1655−1660.
(42) Boyd, C. C.; Cheacharoen, R.; Leijtens, T.; McGehee, M. D. Understanding Degradation Mechanisms and Improving Stability of Perovskite Photovoltaics. *Chem. Rev.* **2019**, *119*, 3418−3451.
(43) Busatto, S.; de Mello Donega, C. Magic-Size Semiconductor Nanostructures: Where Does the Magic Come From? *ACS Mater. Au* **2022**, *2*, 237−249.
(44) Raja, S. N.; Bekenstein, Y.; Koc, M. A.; Fischer, S.; Zhang, D.; Lin, L.; Ritchie, R. O.; Yang, P.; Alivisatos, A. P. Encapsulation of Perovskite Nanocrystals into Macroscale Polymer Matrices: Enhanced Stability and Polarization. *ACS Appl. Mater. Interfaces* **2016**, *8*, 35523−35533.
(45) Wu, H.; Chen, Y.; Zhang, W.; Khan, M. S.; Chi, Y. Water-Dispersed Perovskite Nanocube@SiO_2-C18-PC Core−Shell Nanoparticles for Cell Imaging. *ACS Appl. Nano Mater.* **2021**, *4*, 11791−11800.
(46) Liu, B.; Koh, D.; Wang, A.; Schneider, P.; Oh, K. W. Hermetic Encapsulation of Negative-Pressure-Driven PDMS Microfluidic Devices Using Paraffin Wax and Glass. *Microsyst. Technol.* **2018**, *24*, 2035−2043.
(47) de Mello Donegá, C.; Liljeroth, P.; Vanmaekelbergh, D. Physicochemical Evaluation of the Hot-Injection Method, a Synthesis Route for Monodisperse Nanocrystals. *Small* **2005**, *1*, 1152−1162.
(48) Zhang, L.-J.; Shen, X.-C.; Liang, H.; Yao, J.-T. Multiple Families of Magic-Sized ZnSe Quantum Dots via Noninjection One-Pot and Hot-Injection Synthesis. *J. Phys. Chem. C* **2010**, *114*, 21921−21927.
(49) Houk, L. R.; Challa, S. R.; Grayson, B.; Fanson, P.; Datye, A. K. The Definition of "Critical Radius" for a Collection of Nanoparticles Undergoing Ostwald Ripening. *Langmuir* **2009**, *25*, 11225−11227.
(50) Ali, R. F.; Gates, B. D. Synthesis of Lithium Niobate Nanocrystals with Size Focusing through an Ostwald Ripening Process. *Chem. Mater.* **2018**, *30*, 2028−2035.
(51) Wiese, G. R.; Healy, T. W. Effect of Particle Size on Colloid Stability. *Trans. Faraday Soc.* **1970**, *66*, 490.
(52) Permatasari, F. A.; Masitoh, H. E.; Mahen, E. C. S.; Nuryadin, B. W.; Aimon, A. H.; Syah, Y. M.; Iskandar, F. Synergetic Effect of the Surface Ligand and SiO_2 Driven Photoluminescence Stabilization of the $CH_3NH_3PbBr_3$ Perovskite Magic-Sized Clusters. *Sci. Rep.* **2021**, *11*, 22211.
(53) Wu, H.; Lin, S.; Wang, R.; You, X.; Chi, Y. Water-Stable and Ion Exchange-Free Inorganic Perovskite Quantum Dots Encapsulated in Solid Paraffin and Their Application in Light Emitting Diodes. *Nanoscale* **2019**, *11*, 5557−5563.
(54) Yordanov, G. G.; Yoshimura, H.; Dushkin, C. D. Fine Control of the Growth and Optical Properties of CdSe Quantum Dots by Varying the Amount of Stearic Acid in a Liquid Paraffin Matrix. *Colloids Surf., A* **2008**, *322*, 177−182.
(55) Liu, S.; Yuan, L.; Zhao, Y.; Chen, Y.; Xiang, W.; Liang, X. Water-Stable All-Inorganic $CsPb_{1-X}Sn_XBr_2I$ Perovskite Quantum Dots Encapsulated in Paraffin for White Light-Emitting Diodes. *J. Alloys Compd.* **2019**, *806*, 1022−1028.
(56) Peukert, W.; Schwarzer, H.-C.; Stenger, F. Control of Aggregation in Production and Handling of Nanoparticles. *Chem. Eng. Process.* **2005**, *44*, 245−252.
(57) Govender, K.; Boyle, D. S.; Kenway, P. B.; O'Brien, P. Understanding the Factors That Govern the Deposition and Morphology of Thin Films of ZnO from Aqueous Solution. *J. Mater. Chem.* **2004**, *14*, 2575−2591.
(58) Voorhees, P. W. The Theory of Ostwald Ripening. *J. Stat. Phys.* **1985**, *38*, 231−252.
(59) Baranov, D.; Lynch, M. J.; Curtis, A. C.; Carollo, A. R.; Douglass, C. R.; Mateo-Tejada, A. M.; Jonas, D. M. Purification of Oleylamine for Materials Synthesis and Spectroscopic Diagnostics for Trans Isomers. *Chem. Mater.* **2019**, *31*, 1223−1230.
(60) Liu, F.; Wang, F.; Hansen, K. R.; Zhu, X.-Y. Bimodal Bandgaps in Mixed Cesium Methylammonium Lead Bromide Perovskite Single Crystals. *J. Phys. Chem. C* **2019**, *123*, 14865−14870.
(61) Songvilay, M.; Wang, Z.; Sakai, V. G.; Guidi, T.; Bari, M.; Ye, Z.-G.; Xu, G.; Brown, K. L.; Gehring, P. M.; Stock, C. Decoupled Molecular and Inorganic Framework Dynamics in $CH_3NH_3PbCl_3$. *Phys. Rev. Mater.* **2019**, *3*, 125406.
(62) Mashiyama, H.; Kawamura, Y.; Kubota, Y. The Anti-Polar Structure of $CH_3NH_3PbBr_3$. *J. Korean Phys. Soc.* **2007**, *51*, 850.
(63) Antanovich, A.; Achtstein, W.; Prudnikau, A.; Bhaskar, A.; Gurin, P.; Molinari, V.; Artemyev, M.; Artemyev, M. A Strain-Induced Exciton Transition Energy Shift in CdSe Nanoplatelets: The Impact of an Organic Ligand Shell. *Nanoscale* **2017**, *9*, 18042−18053.
(64) Gao, Y.; Wu, Y.; Lu, H.; Chen, C.; Liu, Y.; Bai, X.; Yang, L.; Yu, W. W.; Dai, Q.; Zhang, Y. $CsPbBr_3$ Perovskite Nanoparticles as Additive for Environmentally Stable Perovskite Solar Cells with 20.46% Efficiency. *Nano Energy* **2019**, *59*, 517−526.
(65) Grin, J.; Burkhardt, U.; Ellner, M.; Peters, K. Crystal Structure of Orthorhombic Co_4Al_{13}. *J. Alloys Compd.* **1994**, *206*, 243−247.
(66) Zhou, Y.; Sun, X.; Zhong, K.; Evans, D. G.; Lin, Y.; Duan, X. Control of Surface Defects and Agglomeration Mechanism of Layered Double Hydroxide Nanoparticles. *Ind. Eng. Chem. Res.* **2012**, *51*, 4215−4221.
(67) Smart, T. J.; Takenaka, H.; Pham, T. A.; Tan, L. Z.; Zhang, J. Z.; Ogitsu, T.; Ping, Y. Enhancing Defect Tolerance with Ligands at the Surface of Lead Halide Perovskites. *J. Phys. Chem. Lett.* **2021**, *12*, 6299−6304.
(68) Dibbell, R. S.; Youker, D. G.; Watson, D. F. Excited-State Electron Transfer from CdS Quantum Dots to TiO_2 Nanoparticles via Molecular Linkers with Phenylene Bridges. *J. Phys. Chem. C* **2009**, *113*, 18643−18651.

https://doi.org/10.1021/acs.jpcc.2c08645
J. Phys. Chem. C 2023, 127, 3367−3376

(69) Xu, K.; Vickers, E. T.; Rao, L.; Lindley, S. A.; Allen, A. C.; Luo, B.; Li, X.; Zhang, J. Z. Synergistic Surface Passivation of $CH_3NH_3PbBr_3$ Perovskite Quantum Dots with Phosphonic Acid and (3-Aminopropyl)Triethoxysilane. *Chem.—Eur. J.* **2019**, *25*, 5014−5021.

https://doi.org/10.1021/acs.jpcc.2c08645
J. Phys. Chem. C 2023, 127, 3367−3376